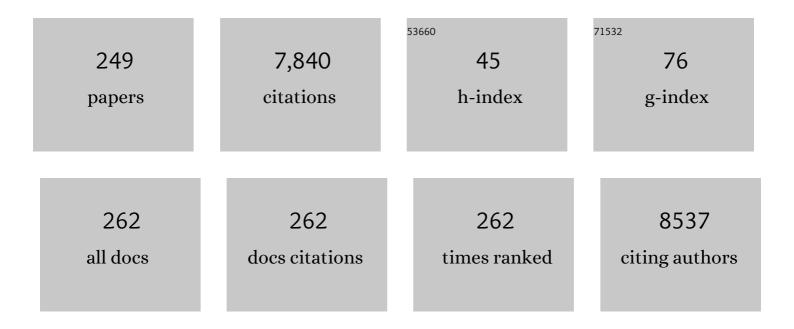
Jae Sung Lee

List of Publications by Year in descending order

Source: https://exaly.com/author-pdf/1255825/publications.pdf Version: 2024-02-01



IAE SUNCLEE

#	Article	IF	CITATIONS
1	Cross-modal plasticity and cochlear implants. Nature, 2001, 409, 149-150.	13.7	575
2	Increased Occupancy of Dopamine Receptors in Human Striatum during Cue-Elicited Cocaine Craving. Neuropsychopharmacology, 2006, 31, 2716-2727.	2.8	280
3	Initial Results of Simultaneous PET/MRI Experiments with an MRI-Compatible Silicon Photomultiplier PET Scanner. Journal of Nuclear Medicine, 2012, 53, 608-614.	2.8	214
4	Tumor-Associated Macrophages Enhance Tumor Hypoxia and Aerobic Glycolysis. Cancer Research, 2019, 79, 795-806.	0.4	188
5	Posterior cingulate cortex atrophy and regional cingulum disruption in mild cognitive impairment and Alzheimer's disease. Neurobiology of Aging, 2010, 31, 772-779.	1.5	178
6	Comparison of Segmentation-Based Attenuation Correction Methods for PET/MRI: Evaluation of Bone and Liver Standardized Uptake Value with Oncologic PET/CT Data. Journal of Nuclear Medicine, 2012, 53, 1878-1882.	2.8	178
7	Neural correlates of clinical symptoms and cognitive dysfunctions in obsessive–compulsive disorder. Psychiatry Research - Neuroimaging, 2003, 122, 37-47.	0.9	173
8	Performance Measurement of the microPET Focus 120 Scanner. Journal of Nuclear Medicine, 2007, 48, 1527-1535.	2.8	161
9	Computed tomography super-resolution using deep convolutional neural network. Physics in Medicine and Biology, 2018, 63, 145011.	1.6	155
10	Positron emission tomography (PET) detectors with depth-of- interaction (DOI) capability. Biomedical Engineering Letters, 2011, 1, 70-81.	2.1	136
11	Differences in δ- and μ-Opioid Receptor Blockade Measured by Positron Emission Tomography in Naltrexone-Treated Recently Abstinent Alcohol-Dependent Subjects. Neuropsychopharmacology, 2008, 33, 653-665.	2.8	133
12	Metabolic connectivity by interregional correlation analysis using statistical parametric mapping (SPM) and FDG brain PET; methodological development and patterns of metabolic connectivity in adults. European Journal of Nuclear Medicine and Molecular Imaging, 2008, 35, 1681-1691.	3.3	131
13	Improving the Accuracy of Simultaneously Reconstructed Activity and Attenuation Maps Using Deep Learning. Journal of Nuclear Medicine, 2018, 59, 1624-1629.	2.8	124
14	Regional cerebral perfusion abnormalities in attention deficit/hyperactivity disorder. European Archives of Psychiatry and Clinical Neuroscience, 2002, 252, 219-225.	1.8	119
15	Regional cerebral blood flow in children with attention deficit hyperactivity disorder: Comparison before and after methylphenidate treatment. Human Brain Mapping, 2005, 24, 157-164.	1.9	108
16	Prediction of the Clinical Outcome of Pediatric Moyamoya Disease With Postoperative Basal/Acetazolamide Stress Brain Perfusion SPECT After Revascularization Surgery. Stroke, 2005, 36, 1485-1489.	1.0	107
17	Generation of PET Attenuation Map for Whole-Body Time-of-Flight ¹⁸ F-FDG PET/MRI Using a Deep Neural Network Trained with Simultaneously Reconstructed Activity and Attenuation Maps. Journal of Nuclear Medicine, 2019, 60, 1183-1189.	2.8	104
18	Presynaptic Dopamine Capacity in Patients with Treatment-Resistant Schizophrenia Taking Clozapine: An [18F]DOPA PET Study. Neuropsychopharmacology, 2017, 42, 941-950.	2.8	98

#	Article	IF	CITATIONS
19	Acute manganese administration alters dopamine transporter levels in the non-human primate striatum. NeuroToxicology, 2006, 27, 229-236.	1.4	87
20	Development of Small-Animal PET Prototype Using Silicon Photomultiplier (SiPM): Initial Results of Phantom and Animal Imaging Studies. Journal of Nuclear Medicine, 2011, 52, 572-579.	2.8	86
21	Methylphenidate increased regional cerebral blood flow in subjects with attention deficit/hyperactivity disorder. Yonsei Medical Journal, 2001, 42, 19.	0.9	79
22	Ictal SPECT in neocortical epilepsies: clinical usefulness and factors affecting the pattern of hyperperfusion. Neuroradiology, 2006, 48, 678-684.	1.1	77
23	Brain single photon emission computed tomography findings in depressive pseudodementia patients. Journal of Affective Disorders, 2002, 69, 159-166.	2.0	76
24	Dual-Phase Tapped-Delay-Line Time-to-Digital Converter With On-the-Fly Calibration Implemented in 40 nm FPGA. IEEE Transactions on Biomedical Circuits and Systems, 2016, 10, 231-242.	2.7	75
25	Time-to-Digital Converter Using a Tuned-Delay Line Evaluated in 28-, 40-, and 45-nm FPGAs. IEEE Transactions on Instrumentation and Measurement, 2016, 65, 1678-1689.	2.4	72
26	Small Animal Imaging in Drug Development. Current Pharmaceutical Design, 2005, 11, 3247-3272.	0.9	68
27	A Four-Layer DOI Detector With a Relative Offset for Use in an Animal PET System. IEEE Transactions on Nuclear Science, 2010, 57, 976-981.	1.2	67
28	Quantification of F-18 FDG PET Images in Temporal Lobe Epilepsy Patients Using Probabilistic Brain Atlas. NeuroImage, 2001, 14, 1-6.	2.1	65
29	Development of Korean Standard Brain Templates. Journal of Korean Medical Science, 2005, 20, 483.	1.1	65
30	Simultaneous Multiparametric PET/MRI with Silicon Photomultiplier PET and Ultra-High-Field MRI for Small-Animal Imaging. Journal of Nuclear Medicine, 2016, 57, 1309-1315.	2.8	64
31	Tractography-guided statistics (TGIS) in diffusion tensor imaging for the detection of gender difference of fiber integrity in the midsagittal and parasagittal corpora callosa. NeuroImage, 2007, 36, 606-616.	2.1	61
32	Continuous depth-of-interaction measurement in a single-layer pixelated crystal array using a single-ended readout. Physics in Medicine and Biology, 2013, 58, 1269-1282.	1.6	61
33	Deep-dose: a voxel dose estimation method using deep convolutional neural network for personalized internal dosimetry. Scientific Reports, 2019, 9, 10308.	1.6	61
34	Diagnostic performance of 18F-FDG PET and ictal 99mTc-HMPAO SPET in pediatric temporal lobe epilepsy: Quantitative analysis by statistical parametric mapping, statistical probabilistic anatomical map, and subtraction ictal SPET. Seizure: the Journal of the British Epilepsy Association, 2005, 14, 213-220.	0.9	58
35	A Review of Deep-Learning-Based Approaches for Attenuation Correction in Positron Emission Tomography. IEEE Transactions on Radiation and Plasma Medical Sciences, 2021, 5, 160-184.	2.7	58
36	PET evidence of neuroplasticity in adult auditory cortex of postlingual deafness. Journal of Nuclear Medicine, 2003, 44, 1435-9.	2.8	56

#	Article	IF	CITATIONS
37	Regional Cerebral Blood Flow Abnormalities Associated With Apathy and Depression in Alzheimer Disease. Alzheimer Disease and Associated Disorders, 2012, 26, 217-224.	0.6	55
38	Topographic Patterns of Brain Functional Impairment Progression According to Clinical Severity Staging in 116 Alzheimer Disease Patients: FDG-PET Study. Alzheimer Disease and Associated Disorders, 2007, 21, 77-84.	0.6	52
39	An Investigation Into the Use of Geiger-Mode Solid-State Photomultipliers for Simultaneous PET and MRI Acquisition. IEEE Transactions on Nuclear Science, 2008, 55, 882-888.	1.2	52
40	Whole-Body Distribution and Radiation Dosimetry of ⁶⁸ Ga-NOTA-RGD, a Positron Emission Tomography Agent for Angiogenesis Imaging. Cancer Biotherapy and Radiopharmaceuticals, 2012, 27, 65-71.	0.7	52
41	Putaminal serotonergic innervation. Neurology, 2015, 85, 853-860.	1.5	51
42	The relationship between antipsychotic D2 occupancy and change in frontal metabolism and working memory. Psychopharmacology, 2013, 227, 221-229.	1.5	49
43	Evaluation of a silicon photomultiplier PET insert for simultaneous PET and MR imaging. Medical Physics, 2015, 43, 72-83.	1.6	49
44	Disparity of Perfusion and Glucose Metabolism of Epileptogenic Zones in Temporal Lobe Epilepsy Demonstrated by SPM/SPAM Analysis on 15 O Water PET, [18 F]FDGâ€PET, and [99m Tc]â€HMPAO SPECT. Epilepsia, 2001, 42, 1515-1522.	2.6	48
45	Dissociation of Working Memory Processing Associated with Native and Second Languages: PET Investigation. NeuroImage, 2002, 15, 879-891.	2.1	47
46	Frontal Dysfunction Underlies Depressive Syndrome in Alzheimer Disease: A FDG-PET Study. American Journal of Geriatric Psychiatry, 2006, 14, 625-628.	0.6	46
47	Design and simulation of a novel method for determining depth-of-interaction in a PET scintillation crystal array using a single-ended readout by a multi-anode PMT. Physics in Medicine and Biology, 2010, 55, 3827-3841.	1.6	46
48	A Dual-Ended Readout Detector Using a Meantime Method for SiPM TOF-DOI PET. IEEE Transactions on Nuclear Science, 2015, 62, 1935-1943.	1.2	46
49	Adaptive template generation for amyloid PET using a deep learning approach. Human Brain Mapping, 2018, 39, 3769-3778.	1.9	46
50	Integrated Whole Body MR/PET: Where Are We?. Korean Journal of Radiology, 2015, 16, 32.	1.5	44
51	SiPM-PET with a short optical fiber bundle for simultaneous PET-MR imaging. Physics in Medicine and Biology, 2012, 57, 3869-3883.	1.6	42
52	Extrastriatal dopaminergic changes in Parkinson's disease patients with impulse control disorders. Journal of Neurology, Neurosurgery and Psychiatry, 2014, 85, 23-30.	0.9	42
53	Videostrobokymography: A New Method for the Quantitative Analysis of Vocal Fold Vibration. Laryngoscope, 1999, 109, 1859-1863.	1.1	41
54	Kinetic Modeling of 3′-Deoxy-3′-18F-Fluorothymidine for Quantitative Cell Proliferation Imaging in Subcutaneous Tumor Models in Mice. Journal of Nuclear Medicine, 2008, 49, 2057-2066.	2.8	40

#	Article	IF	CITATIONS
55	[11C]-(R)-PK11195 positron emission tomography in patients with complex regional pain syndrome. Medicine (United States), 2017, 96, e5735.	0.4	40
56	Whole-Body Voxel-Based Personalized Dosimetry: The Multiple Voxel S-Value Approach for Heterogeneous Media with Nonuniform Activity Distributions. Journal of Nuclear Medicine, 2018, 59, 1133-1139.	2.8	40
57	Measurement of Glomerular Filtration Rate using Quantitative SPECT/CT and Deep-learning-based Kidney Segmentation. Scientific Reports, 2019, 9, 4223.	1.6	40
58	Effect of worry on regional cerebral blood flow in nonanxious subjects. Psychiatry Research - Neuroimaging, 2005, 140, 259-269.	0.9	39
59	Highly Integrated FPGA-Only Signal Digitization Method Using Single-Ended Memory Interface Input Receivers for Time-of-Flight PET Detectors. IEEE Transactions on Biomedical Circuits and Systems, 2018, 12, 1401-1409.	2.7	38
60	The relationship between regional cerebral blood flow and response to methylphenidate in children with attention-deficit hyperactivity disorder: Comparison between non-responders to methylphenidate and responders. Journal of Psychiatric Research, 2007, 41, 459-465.	1.5	37
61	Neural Correlates of the Clock Drawing Test Performance in Alzheimer's Disease: A FDG-PET Study. Dementia and Geriatric Cognitive Disorders, 2008, 26, 306-313.	0.7	37
62	Discrimination of normal aging, MCI and AD with multimodal imaging measures on the medial temporal lobe. Psychiatry Research - Neuroimaging, 2010, 183, 237-243.	0.9	37
63	Radiation Dose from Whole-Body F-18 Fluorodeoxyglucose Positron Emission Tomography/Computed Tomography: Nationwide Survey in Korea. Journal of Korean Medical Science, 2016, 31, S69.	1.1	37

64 Whole-Brain Diffusion-Tensor Changes in Parkinsonian Patients with Impulse Control Disorders.

#	Article	IF	CITATIONS
73	A depth-of-interaction PET detector using a stair-shaped reflector arrangement and a single-ended scintillation light readout. Physics in Medicine and Biology, 2017, 62, 465-483.	1.6	30
74	Different uptake of 99mTc-ECD and 99mTc-HMPAO in the same brains: analysis by statistical parametric mapping. European Journal of Nuclear Medicine and Molecular Imaging, 2001, 28, 191-197.	2.2	29
75	Probabilistic map of blood flow distribution in the brain from the internal carotid artery. NeuroImage, 2004, 23, 1422-1431.	2.1	29
76	Voxel-based statistical analysis of cerebral glucose metabolism in the rat cortical deafness model by 3D reconstruction of brain from autoradiographic images. European Journal of Nuclear Medicine and Molecular Imaging, 2005, 32, 696-701.	3.3	29
77	Depth-of-interaction measurement in a single-layer crystal array with a single-ended readout using digital silicon photomultiplier. Physics in Medicine and Biology, 2015, 60, 6495-6514.	1.6	29
78	Hybrid charge division multiplexing method for silicon photomultiplier based PET detectors. Physics in Medicine and Biology, 2017, 62, 4390-4405.	1.6	29
79	Localization of epileptogenic zones in F-18 FDG brain PET of patients with temporal lobe epilepsy using artificial neural network. IEEE Transactions on Medical Imaging, 2000, 19, 347-355.	5.4	28
80	Superiority of HMPAO Ictal SPECT to ECD Ictal SPECT in Localizing the Epileptogenic Zone. Epilepsia, 2002, 43, 263-269.	2.6	28
81	Predicting Brain Occupancy from Plasma Levels using PET: Superiority of Combining Pharmacokinetics with Pharmacodynamics while Modeling the Relationship. Journal of Cerebral Blood Flow and Metabolism, 2012, 32, 759-768.	2.4	28
82	Signal encoding method for a time-of-flight PET detector using a silicon photomultiplier array. Nuclear Instruments and Methods in Physics Research, Section A: Accelerators, Spectrometers, Detectors and Associated Equipment, 2014, 761, 39-45.	0.7	28
83	Clinical Applications of Simultaneous PET/MR Imaging Using (<i>R</i>)-[¹¹ C]-Verapamil with Cyclosporin A: Preliminary Results on a Surrogate Marker of Drug-Resistant Epilepsy. American Journal of Neuroradiology, 2016, 37, 600-606.	1.2	28
84	MRI-Based Attenuation Correction for PET/MRI Using Multiphase Level-Set Method. Journal of Nuclear Medicine, 2016, 57, 587-593.	2.8	28
85	The relationship between dopamine receptor blockade and cognitive performance in schizophrenia: a [11C]-raclopride PET study with aripiprazole. Translational Psychiatry, 2018, 8, 87.	2.4	28
86	Efficacy assessment of cerebral arterial bypass surgery using statistical parametric mapping and probabilistic brain atlas on basal/acetazolamide brain perfusion SPECT. Journal of Nuclear Medicine, 2004, 45, 202-6.	2.8	28
87	Age-associated changes of cerebral glucose metabolic activity in both male and female deaf children: parametric analysis using objective volume of interest and voxel-based mapping. NeuroImage, 2004, 22, 1543-1553.	2.1	27
88	Probabilistic Anatomic Mapping of Cerebral Blood Flow Distribution of the Middle Cerebral Artery. Journal of Nuclear Medicine, 2008, 49, 39-43.	2.8	27
89	A method for assessing the regional vibratory pattern of vocal folds by analysing the video recording of stroboscopy. Medical and Biological Engineering and Computing, 2001, 39, 273-278.	1.6	26
90	Gap compensation during PET image reconstruction by constrained, total variation minimization. Medical Physics, 2012, 39, 589-602.	1.6	26

#	Article	IF	CITATIONS
91	Resolution recovery reconstruction for a Compton camera. Physics in Medicine and Biology, 2013, 58, 2823-2840.	1.6	26
92	Two approaches to implementing projector–backprojector pairs for 3D reconstruction from Compton scattered data. Nuclear Instruments and Methods in Physics Research, Section A: Accelerators, Spectrometers, Detectors and Associated Equipment, 2007, 571, 255-258.	0.7	25
93	Development of a front-end analog circuit for multi-channel SiPM readout and performance verification for various PET detector designs. Nuclear Instruments and Methods in Physics Research, Section A: Accelerators, Spectrometers, Detectors and Associated Equipment, 2013, 703, 38-44.	0.7	25
94	Feasibility and kinetic characteristics of 68Ga-NOTA-RGD PET for in vivo atherosclerosis imaging. Annals of Nuclear Medicine, 2013, 27, 847-854.	1.2	25
95	Timing Performance Study of New Fast PMTs With LYSO for Time-of-Flight PET. IEEE Transactions on Nuclear Science, 2013, 60, 30-37.	1.2	25
96	Development and applications of a software for Functional Image Registration (FIRE). Computer Methods and Programs in Biomedicine, 2005, 78, 157-164.	2.6	24
97	Development of double-scattering-type Compton camera with double-sided silicon strip detectors and NaI(TI) scintillation detector. Nuclear Instruments and Methods in Physics Research, Section A: Accelerators, Spectrometers, Detectors and Associated Equipment, 2010, 615, 333-339.	0.7	24
98	Fully three-dimensional OSEM-based image reconstruction for Compton imaging using optimized ordering schemes. Physics in Medicine and Biology, 2010, 55, 5007-5027.	1.6	24
99	Segmentation-Based MR Attenuation Correction Including Bones Also Affects Quantitation in Brain Studies: An Initial Result of ¹⁸ F-FP-CIT PET/MR for Patients with Parkinsonism. Journal of Nuclear Medicine, 2014, 55, 1617-1622.	2.8	24
100	Development of FPGA-based coincidence units with veto function. Biomedical Engineering Letters, 2011, 1, 27-31.	2.1	23
101	Crystal surface and reflector optimization for the SiPM-based dual-ended readout TOF-DOI PET detector. Biomedical Physics and Engineering Express, 2020, 6, 065028.	0.6	23
102	Technical Advances in Current PET and Hybrid Imaging Systems. The Open Nuclear Medicine Journal, 2010, 2, 192-208.	0.2	23
103	Assessment of Cerebral Glucose Metabolism in Cat Deafness Model: Strategies for Improving the Voxel-Based Statistical Analysis for Animal PET Studies. Molecular Imaging and Biology, 2008, 10, 154-161.	1.3	22
104	Highly multiplexed SiPM signal readout for brain-dedicated TOF-DOI PET detectors. Physica Medica, 2019, 68, 117-123.	0.4	22
105	SimPET: a Preclinical PET Insert for Simultaneous PET/MR Imaging. Molecular Imaging and Biology, 2020, 22, 1208-1217.	1.3	22
106	Scalable electronic readout design for a 100 ps coincidence time resolution TOF-PET system. Physics in Medicine and Biology, 2021, 66, 085005.	1.6	22
107	Proofâ€ofâ€concept prototype timeâ€ofâ€flight <scp>PET</scp> system based on highâ€quantumâ€efficiency multianode <scp>PMT</scp> s. Medical Physics, 2017, 44, 5314-5324.	1.6	21
108	Self-supervised PET Denoising. Nuclear Medicine and Molecular Imaging, 2020, 54, 299-304.	0.6	21

#	Article	IF	CITATIONS
109	Performance characterization of high quantum efficiency metal package photomultiplier tubes for timeâ€ofâ€flight and highâ€resolution PET applications. Medical Physics, 2015, 42, 510-520.	1.6	20
110	Deep learning-Based 3D inpainting of brain MR images. Scientific Reports, 2021, 11, 1673.	1.6	20
111	Changes of 2-deoxyglucose uptake in the rat auditory pathway after bilateral ablation of the cochlea. Hearing Research, 2004, 196, 33-38.	0.9	19
112	Single transmission-line readout method for silicon photomultiplier based time-of-flight and depth-of-interaction PET. Physics in Medicine and Biology, 2017, 62, 2194-2207.	1.6	19
113	Prototype pre-clinical PET scanner with depth-of-interaction measurements using single-layer crystal array and single-ended readout. Physics in Medicine and Biology, 2017, 62, 3983-3996.	1.6	19
114	Abnormal neuroinflammation in fibromyalgia and CRPS using [11C]-(R)-PK11195 PET. PLoS ONE, 2021, 16, e0246152.	1.1	19
115	The usefulness of repeated ictal SPET for the localization of epileptogenic zones in intractable epilepsy. European Journal of Nuclear Medicine and Molecular Imaging, 2002, 29, 607-614.	3.3	18
116	FDG-PET for Pharmacodynamic Assessment of the Fatty Acid Synthase Inhibitor C75 in an Experimental Model of Lung Cancer. Pharmaceutical Research, 2007, 24, 1202-1207.	1.7	18
117	Delay grid multiplexing: simple time-based multiplexing and readout method for silicon photomultipliers. Physics in Medicine and Biology, 2016, 61, 7113-7135.	1.6	18
118	Recovery of inter-detector and inter-crystal scattering in brain PET based on LSO and GAGG crystals. Physics in Medicine and Biology, 2020, 65, 195005.	1.6	18
119	Loss of asymmetry in D ₂ receptors of putamen in unaffected family members at increased genetic risk for schizophrenia. Acta Psychiatrica Scandinavica, 2008, 118, 200-208.	2.2	17
120	A New Image-Based Stroke Registry Containing Quantitative Magnetic Resonance Imaging Data. Cerebrovascular Diseases, 2011, 32, 567-576.	0.8	17
121	Advances in imaging instrumentation for nuclear cardiology. Journal of Nuclear Cardiology, 2019, 26, 543-556.	1.4	17
122	Silicon photomultiplier signal readout and multiplexing techniques for positron emission tomography: a review. Biomedical Engineering Letters, 2022, 12, 263-283.	2.1	17
123	Cross-modal and compensatory plasticity in adult deafened cats: A longitudinal PET study. Brain Research, 2010, 1354, 85-90.	1.1	16
124	Monte Carlo simulation of a four-layer DOI detector with relative offset in animal PET. Nuclear Instruments and Methods in Physics Research, Section A: Accelerators, Spectrometers, Detectors and Associated Equipment, 2011, 626-627, 43-50.	0.7	16
125	Recent Advances in Hybrid Molecular Imaging Systems. Seminars in Musculoskeletal Radiology, 2014, 18, 103-122.	0.4	16
126	Evaluation of a fast photomultiplier tube for time-of-flight PET. Biomedical Engineering Letters, 2011, 1, 174-179.	2.1	15

#	Article	IF	CITATIONS
127	Feasibility of PET Template-Based Analysis on F-18 FP-CIT PET in Patients with De Novo Parkinson's Disease. Nuclear Medicine and Molecular Imaging, 2013, 47, 73-80.	0.6	15
128	Preclinical voxel-based dosimetry through GATE Monte Carlo simulation using PET/CT imaging of mice. Physics in Medicine and Biology, 2019, 64, 095007.	1.6	15
129	Frontostriatal functional connectivity and striatal dopamine synthesis capacity in schizophrenia in terms of antipsychotic responsiveness: an [¹⁸ F]DOPA PET and fMRI study. Psychological Medicine, 2019, 49, 2533-2542.	2.7	15
130	Dopamine dysregulation in psychotic relapse after antipsychotic discontinuation: an [18F]DOPA and [11C]raclopride PET study in first-episode psychosis. Molecular Psychiatry, 2021, 26, 3476-3488.	4.1	15
131	[18F]CB251 PET/MR imaging probe targeting translocator protein (TSPO) independent of its Polymorphism in a Neuroinflammation Model. Theranostics, 2020, 10, 9315-9331.	4.6	15
132	Synthetic CT generation from weakly paired MR images using cycle-consistent GAN for MR-guided radiotherapy. Biomedical Engineering Letters, 2021, 11, 263-271.	2.1	15
133	Generation of parametric image of regional myocardial blood flow using H(2)(15)O dynamic PET and a linear least-squares method. Journal of Nuclear Medicine, 2005, 46, 1687-95.	2.8	15
134	Experimental performance of double-scattering Compton camera with anthropomorphic phantom. Journal of Instrumentation, 2011, 6, C01024-C01024.	0.5	14
135	A novel compensation method for the anode gain non-uniformity of multi-anode photomultiplier tubes. Physics in Medicine and Biology, 2012, 57, 191-207.	1.6	14
136	Performance Evaluation of SimPET-X, a PET Insert for Simultaneous Mouse Total-Body PET/MR Imaging. Molecular Imaging and Biology, 2021, 23, 703-713.	1.3	14
137	Development and Performance Evaluation of a Time-of-Flight Positron Emission Tomography Detector Based on a High-Quantum-Efficiency Multi-Anode Photomultiplier Tube. IEEE Transactions on Nuclear Science, 2016, 63, 44-51.	1.2	13
138	Novel inter-crystal scattering event identification method for PET detectors. Physics in Medicine and Biology, 2018, 63, 115015.	1.6	13
139	SiPM-based dual-ended-readout DOI-TOF PET module based on mean-time method. Journal of Instrumentation, 2019, 14, P02023-P02023.	0.5	13
140	Voxel-Based Dosimetry of Iron Oxide Nanoparticle-Conjugated 177Lu-Labeled Folic Acid Using SPECT/CT Imaging of Mice. Molecular Pharmaceutics, 2019, 16, 1498-1506.	2.3	13
141	Inter-crystal scattering recovery of light-sharing PET detectors using convolutional neural networks. Physics in Medicine and Biology, 2021, 66, 185004.	1.6	13
142	The use of healthy volunteers instead of patients to inform drug dosing studies: a [11C]raclopride PET study. Psychopharmacology, 2011, 217, 515-523.	1.5	12
143	Validation of Simple Quantification Methods for 18F-FP-CIT PET Using Automatic Delineation of Volumes of Interest Based on Statistical Probabilistic Anatomical Mapping and Isocontour Margin Setting. Nuclear Medicine and Molecular Imaging, 2012, 46, 254-260.	0.6	12
144	Quantitative positron emission tomography imaging of angiogenesis in rats with forelimb ischemia using 68Ga-NOTA-c(RGDyK). Angiogenesis, 2013, 16, 837-846.	3.7	12

#	Article	IF	CITATIONS
145	Translating amyloid PET of different radiotracers by a deep generative model for interchangeability. NeuroImage, 2021, 232, 117890.	2.1	12
146	Fusion of coregistered cross-modality images using a temporally alternating display method. Medical and Biological Engineering and Computing, 2000, 38, 127-132.	1.6	11
147	CIS: A GUI-Based Software System for Monte Carlo Simulation of Compton Camera. Nuclear Technology, 2009, 168, 55-60.	0.7	11
148	Bipolar analog signal multiplexing for position-sensitive PET block detectors. Physics in Medicine and Biology, 2014, 59, 7835-7846.	1.6	11
149	Quantitative salivary gland SPECT/CT using deep convolutional neural networks. Scientific Reports, 2021, 11, 7842.	1.6	11
150	Data-driven respiratory phase-matched PET attenuation correction without CT. Physics in Medicine and Biology, 2021, 66, 115009.	1.6	11
151	Comparison of deep learning-based emission-only attenuation correction methods for positron emission tomography. European Journal of Nuclear Medicine and Molecular Imaging, 2022, 49, 1833-1842.	3.3	11
152	Multiple Linear Analysis Methods for the Quantification of Irreversibly Binding Radiotracers. Journal of Cerebral Blood Flow and Metabolism, 2008, 28, 1965-1977.	2.4	10
153	Taq1A polymorphism in the dopamine D2 receptor gene predicts brain metabolic response to aripiprazole in healthy male volunteers. Pharmacogenetics and Genomics, 2008, 18, 91-97.	0.7	10
154	Feasibility of Template-Guided Attenuation Correction in Cat Brain PET Imaging. Molecular Imaging and Biology, 2010, 12, 250-258.	1.3	10
155	Multitracing Capability of Double-Scattering Compton Imager With NaI(Tl) Scintillator Absorber. IEEE Transactions on Nuclear Science, 2010, 57, 1420-1425.	1.2	10
156	Association between partial-volume corrected SUVmax and Oncotype DX recurrence score in early-stage, ER-positive/HER2-negative invasive breast cancer. European Journal of Nuclear Medicine and Molecular Imaging, 2016, 43, 1574-1584.	3.3	10
157	Changes in the Heterogeneity of Cerebral Glucose Metabolism with Healthy Aging: Quantitative Assessment by Fractal Analysis. Journal of Neuroimaging, 2004, 14, 350-356.	1.0	9
158	Parametric image of myocardial blood flow generated from dynamic H2 15O PET using factor analysis and cluster analysis. Medical and Biological Engineering and Computing, 2005, 43, 678-685.	1.6	9
159	Recent advances in parametric neuroreceptor mapping with dynamic PET: basic concepts and graphical analyses. Neuroscience Bulletin, 2014, 30, 733-754.	1.5	9
160	Regional Differences in Serotonin Transporter Occupancy by Escitalopram: An [11C]DASB PK-PD Study. Clinical Pharmacokinetics, 2017, 56, 371-381.	1.6	9
161	Multi-atlas cardiac PET segmentation. Physica Medica, 2019, 58, 32-39.	0.4	9
162	Time-based signal sampling using sawtooth-shaped threshold. Physics in Medicine and Biology, 2019, 64, 125020.	1.6	9

#	Article	IF	CITATIONS
163	Preclinical Voxel-Based Dosimetry in Theranostics: a Review. Nuclear Medicine and Molecular Imaging, 2020, 54, 86-97.	0.6	9
164	SiPM signal readout for inter-crystal scatter event identification in PET detectors. Physics in Medicine and Biology, 2020, 65, 205010.	1.6	9
165	Positron emission tomography during transcranial magnetic stimulation does not require μ-metal shielding. Neurolmage, 2003, 19, 1812-1819.	2.1	8
166	Reproducibility of the kinetic analysis of 3′-deoxy-3′-[18F]fluorothymidine positron emission tomography in mouse tumor models. Nuclear Medicine and Biology, 2009, 36, 711-719.	0.3	8
167	Calculating Occupancy when One does not have Baseline: A Comparison of Different Options. Journal of Cerebral Blood Flow and Metabolism, 2011, 31, 1760-1767.	2.4	8
168	Comparative Assessment of Parametric Neuroreceptor Mapping Approaches Based on the Simplified Reference Tissue Model Using [¹¹ C]ABP688 PET. Journal of Cerebral Blood Flow and Metabolism, 2015, 35, 2098-2108.	2.4	8
169	Comparator-less PET data acquisition system using single-ended memory interface input receivers of FPGA. Physics in Medicine and Biology, 2020, 65, 155007.	1.6	8
170	Investigation of Solid-State Photomultipliers for Positron Emission Tomography Scanners. Journal of the Korean Physical Society, 2007, 50, 1332.	0.3	8
171	Non-negative matrix factorization of dynamic images in nuclear medicine. , 0, , .		7
172	Feasibility study on hybrid medical imaging device based on Compton imaging and magnetic resonance imaging. Applied Radiation and Isotopes, 2009, 67, 1412-1415.	0.7	7
173	Assessment of MR-compatibility of SiPM PET insert using short optical fiber bundles for small animal research. Journal of Instrumentation, 2015, 10, P12008-P12008.	0.5	7
174	Joint estimation of activity distribution and attenuation map for TOF-PET using alternating direction method of multiplier. , 2016, , .		7
175	Feasibility of simultaneous 18F-FDG PET/MRI for the quantitative volumetric and metabolic measurements of abdominal fat tissues using fat segmentation. Nuclear Medicine Communications, 2016, 37, 616-622.	0.5	7
176	Achieving reliable coincidence resolving time measurement of PET detectors using multichannel waveform digitizer based on DRS4 chip. Physics in Medicine and Biology, 2018, 63, 24NT02.	1.6	7
177	Comparison of voxel <i>S</i> â€value methods for personalized voxelâ€based dosimetry of ¹⁷⁷ Luâ€DOTATATE. Medical Physics, 2022, 49, 1888-1901.	1.6	7
178	Automatic Lung Cancer Segmentation in [18F]FDG PET/CT Using a Two-Stage Deep Learning Approach. Nuclear Medicine and Molecular Imaging, 2023, 57, 86-93.	0.6	7
179	A Feasibility Study on the Use of Optical Fibers for the Transfer of Scintillation Light to Silicon Photomultipliers. IEEE Transactions on Nuclear Science, 2011, 58, 579-589.	1.2	6
180	Performance of a new accelerating-electrode-equipped fast-time-response PMT coupled with fast LGSO. Physics in Medicine and Biology, 2018, 63, 05NT03.	1.6	6

#	Article	IF	CITATIONS
181	Promotion of Nuclear Medicine-Related Sciences in Developing Countries. Nuclear Medicine and Molecular Imaging, 2019, 53, 73-82.	0.6	6
182	Evaluation of coronary endothelial dysfunction in healthy young smokers: Cold pressor test using [150]H2O PET. Applied Radiation and Isotopes, 2009, 67, 1199-1203.	0.7	5
183	Compartmental modeling and simplified quantification of [11C]sertraline distribution in human brain. Archives of Pharmacal Research, 2012, 35, 1591-1597.	2.7	5
184	Imaging of activated cortical areas after light and electrical stimulation of the rabbit retina: F-18 FDG PET-guided brain mapping. Biomedical Engineering Letters, 2012, 2, 111-117.	2.1	5
185	Evaluation of a FPGA-based Real-Time Coincidence System for High Count Rate PET Scanners. , 2017, , .		5
186	Systematic study on factors influencing the performance of interdetector scatter recovery in smallâ€animal <scp>PET</scp> . Medical Physics, 2018, 45, 3551-3562.	1.6	5
187	Performance Evaluation and Quantitative Accuracy of Multipinhole NanoSPECT/CT Scanner for Theranostic Lu-177 Imaging. Journal of the Korean Physical Society, 2018, 72, 1379-1386.	0.3	5
188	Evaluation of Large-Area Silicon Photomultiplier Arrays for Positron Emission Tomography Systems. Electronics (Switzerland), 2021, 10, 698.	1.8	5
189	Anatomy-guided PET reconstruction using l ₁ bowsher prior. Physics in Medicine and Biology, 2021, 66, 095010.	1.6	5
190	A positron emission tomography microdosing study with sertraline in healthy volunteers. International Journal of Clinical Pharmacology and Therapeutics, 2012, 50, 224-232.	0.3	5
191	Investigation of Electronic Signal Processing Chains for a Prototype TOF-PET System With 100-ps Coincidence Time Resolution. IEEE Transactions on Radiation and Plasma Medical Sciences, 2022, 6, 690-696.	2.7	5
192	Changes in the heterogeneity of cerebral glucose metabolism with healthy aging: quantitative assessment by fractal analysis. , 2004, 14, 350-6.		5
193	Image-level trajectory inference of tau pathology using variational autoencoder for Flortaucipir PET. European Journal of Nuclear Medicine and Molecular Imaging, 2022, 49, 3061-3072.	3.3	5
194	Alteration of functional neuroanatomy of simple object memory in medial temporal lobe epilepsy patients. NeuroReport, 2002, 13, 2475-2481.	0.6	4
195	Performance evaluation of a table-top Compton camera for various detector parameters. Nuclear Instruments and Methods in Physics Research, Section A: Accelerators, Spectrometers, Detectors and Associated Equipment, 2008, 591, 88-91.	0.7	4
196	Three-dimensional edge-preserving regularization for Compton camera reconstruction. , 2008, , .		4
197	Noninvasive bi-graphical analysis for the quantification of slowly reversible radioligand binding. Physics in Medicine and Biology, 2016, 61, 6770-6790.	1.6	4
198	AID – A Novel Method for Improving the Imaging Resolution of a Table-Top Compton Camera. IEEE Transactions on Nuclear Science, 2008, 55, 2527-2530.	1.2	3

#	Article	IF	CITATIONS
199	Spatiotemporal dynamics and functional correlates of evoked neural oscillations with different spectral powers in human visual cortex. Clinical Neurophysiology, 2013, 124, 2248-2256.	0.7	3
200	A strategy to reduce blocky pattern and contrast loss in emission tomography reconstruction with reduced angular sampling and total variation minimization. Biomedical Engineering Letters, 2014, 4, 362-369.	2.1	3
201	Comparative evaluation of the algorithms for parametric mapping of the novel myocardial PET imaging agent 18F-FPTP. Annals of Nuclear Medicine, 2017, 31, 469-479.	1.2	3
202	Therapeutic Effect of Fimasartan in a Rat Model of Myocardial Infarction Evaluated by Cardiac Positron Emission Tomography with [18F]FPTP. Chonnam Medical Journal, 2019, 55, 109.	0.5	3
203	Fully three-dimensional image reconstruction for compton imaging using ordered subsets of conical projection data. , 2007, , .		2
204	Monte Carlo simulations on performance of double-scattering Compton camera. Journal of Instrumentation, 2012, 7, C01009-C01009.	0.5	2
205	Basic Nuclear Physics and Instrumentation. , 2012, , 3-19.		2
206	Automated Analysis of 123I-beta-CIT SPECT Images with Statistical Probabilistic Anatomical Mapping. Nuclear Medicine and Molecular Imaging, 2014, 48, 47-54.	0.6	2
207	Derivation of the scan time requirement for maintaining a consistent PET image quality. Journal of Instrumentation, 2015, 10, P05011-P05011.	0.5	2
208	Innovative Physics and Engineering Research in Nuclear Medicine and Molecular Imaging: A Message from the Associate Editor. Nuclear Medicine and Molecular Imaging, 2015, 49, 249-250.	0.6	2
209	Development of a non-delay line constant fraction discriminator based on the Padé approximant for time-of-flight positron emission tomography scanners. Journal of Instrumentation, 2015, 10, P01005-P01005.	0.5	2
210	Biodistribution and internal radiation dosimetry of a companion diagnostic radiopharmaceutical, [68Ca]PSMA-11, in subcutaneous prostate cancer xenograft model mice. Scientific Reports, 2021, 11, 15263.	1.6	2
211	A temperature-dependent gain compensation technique for positron emission tomography detectors based on a silicon photomultiplier. Physics in Medicine and Biology, 2021, 66, 205015.	1.6	2
212	Relationship Between Ktrans and K1 with Simultaneous Versus Separate MR/PET in Rabbits with VX2 Tumors. Anticancer Research, 2017, 37, 1139-1148.	0.5	2
213	A neural network classifier for the automatic interpretation of epileptogenic zones in F-18FDG brain PET. , 0, , .		1
214	Rectified subspace analysis of dynamic positron emission tomography. , 2002, , .		1
215	Development of quantification software using model-based segmentation of left ventricular myocardium in gated myocardial SPECT. Computer Methods and Programs in Biomedicine, 2006, 83, 43-49.	2.6	1
216	A Clinical Application of Ensemble ICA to the Quantification of Myocardial Blood Flow in Dynamic \$\$ H^{{15}}_{2} O \$\$ PET. Journal of Signal Processing Systems, 2007, 49, 233-241.	1.0	1

#	Article	IF	CITATIONS
217	An axis of rotation alignment system for high-resolution pinhole SPECT imaging. Nuclear Instruments and Methods in Physics Research, Section A: Accelerators, Spectrometers, Detectors and Associated Equipment, 2008, 589, 338-344.	0.7	1
218	Variance-reduction normalization technique for a compton camera system. Journal of Instrumentation, 2011, 6, C01040-C01040.	0.5	1
219	Compton-edge-based energy calibration of double-sided silicon strip detectors in Compton camera. Nuclear Instruments and Methods in Physics Research, Section A: Accelerators, Spectrometers, Detectors and Associated Equipment, 2011, 633, S108-S110.	0.7	1
220	PET/MRI. , 2013, , 373-390.		1
221	Preliminary evaluation of a brain PET insertable to MRI. EJNMMI Physics, 2014, 1, A13.	1.3	1
222	The use of fluorine-18 fluorodeoxyglucose positron emission tomography for imaging human motor neuronal activation in the brain. Experimental and Therapeutic Medicine, 2015, 10, 2126-2130.	0.8	1
223	Design optimization of a small-animal SPECT system using LCSO continuous crystals and micro parallel-hole collimators. Journal of the Korean Physical Society, 2015, 67, 224-231.	0.3	1
224	Musculoskeletal Lesions: Nuclear Medicine Imaging Pitfalls. , 2017, , 951-976.		1
225	Robust nonlinear parameter estimation in tracer kinetic analysis using infinity norm regularization and particle swarm optimization. Physica Medica, 2020, 72, 60-72.	0.4	1
226	Investigation of Analog and Digital Signal Processing Chains for a Prototype TOF-PET System with 100 ps Coincidence Time Resolution. , 2020, , .		1
227	SPATIAL AND ENERGY RESOLUTIONS OF A HEXAGONAL ANIMAL PET SCANNER BASED ON LGSO CRYSTAL AND FLAT-PANEL PMT. Nuclear Engineering and Technology, 2012, 44, 53-60.	1.1	1
228	A time-based single transmission-line readout with position multiplexing. Biomedical Engineering Letters, 2022, 12, 85-95.	2.1	1
229	Computerized densitometric measurement system (CDMS) for the quantitative analysis of diffuse retinal nerve fiber layer atrophy. Journal of Medical Engineering and Technology, 2000, 24, 237-241.	0.8	0
230	Performance evaluation of SIEMENS CTI ECAT EXACT 47 PET scanner USING NEMA NU2-2001. , 0, , .		0
231	Separation of factor images for blood flow estimation in positron emission tomography using ensemble independent component analysis. , 0, , .		0
232	Parametric image of regional bone metabolism using F-18 PET using a multiple linear regression analysis method. , 2007, , .		0
233	Verification of concepts for DOI determination in a three-layer small animal PET. , 2007, , .		0
234	A simplified geometric calibration method for rotating triple head pinhole SPECT system using point source. , 2007, , .		0

Jae Sung Lee

#	Article	IF	CITATIONS
235	A novel method improving the imaging resolution of a table-top Compton camera. , 2007, , .		0
236	Comparative evaluation of three microPET series systems using Monte Carlo simulation: sensitivity and scatter fraction. , 2007, , .		0
237	Comparison of maximal elastance and systolic wall thickening using arterial tonometry and gated myocardial SPECT in patients undergoing coronary artery bypass grafting. Applied Radiation and Isotopes, 2009, 67, 1382-1386.	0.7	0
238	Resolution recoverable statistical listmode reconstruction using depth dependent point spread function for Compton camera. , 2010, , .		0
239	Feasibility study on Compton imaging for visualization of flow patterns using radiotracers. Journal of Instrumentation, 2011, 6, C01023-C01023.	0.5	0
240	Explicit modeling of timing characteristics in Compton camera simulation with Geant4. Nuclear Instruments and Methods in Physics Research, Section A: Accelerators, Spectrometers, Detectors and Associated Equipment, 2011, 633, S274-S275.	0.7	0
241	Tracer Kinetics in Radionanomedicine. Biological and Medical Physics Series, 2018, , 293-310.	0.3	0
242	Biomedical engineering letters' decade-long success. Biomedical Engineering Letters, 2021, 11, 1-2.	2.1	0
243	Efficacy of voxel-based dosimetry map for predicting response to trans-arterial radioembolization therapy for hepatocellular carcinoma. Nuclear Medicine Communications, 2021, Publish Ahead of Print, 1396-1403.	0.5	0
244	Partial Volume Correction of Simulated PET and 18F FDG PET from 14 Normal Brains. , 2002, , 153-157.		0
245	Simultaneous positron emission tomography and magnetic resonance imaging. SPIE Newsroom, 0, , .	0.1	0
246	A Brief History of Nuclear Medicine Physics, Instrumentation, and Data Sciences in Korea. Nuclear Medicine and Molecular Imaging, 2021, 55, 265-284.	0.6	0
247	Studies of a Scalable Electronic Readout Design for a 100 ps Coincidence Time Resolution TOF-PET System. , 2020, , .		0
248	Biomedical Engineering Letters indexed in Science Citation Index Expanded (SCIE). Biomedical Engineering Letters, 2022, 12, 1-1.	2.1	0
249	Purecomb: Poisson Unbiased Risk Estimator Based Ensemble of Self-Supervised Deep Denoisers For Clinical Bone Scan Image. , 2022, , .		0

15